The trichothecene mycotoxin deoxynivalenol facilitates cell-to-cell invasion during wheat-tissue colonisation by *Fusarium graminearum*

Victoria Armer (1, 2), Martin Urban (1), Tom Ashfield (3), Michael J. Deeks (2) and Kim E. Hammond-Kosack *(1)

1. Protecting Crops and the Environment, Rothamsted Research, Harpenden, AL5 2JQ, UK.
2. Biosciences, Geoffrey Pope Building, University of Exeter, Stocker Road, Exeter, EX4 4QD, UK.
3. Crop Health and Protection (CHAP), Rothamsted Research, Harpenden, AL5 2JQ, UK.

*Corresponding author: kim.hammond-kosack@rothamsted.ac.uk

Key words: *Fusarium graminearum*, deoxynivalenol (DON), plasmodesmata, wheat (*Triticum aestivum*), head scab disease

Word count

Abstract: 199

Introduction: 1484

Results: 1562

Discussion: 1711

Experimental Procedures: 1977

Acknowledgements: 117

Table and Figure legends: 1000

Abstract

Fusarium Head Blight (FHB) disease on small grain cereals is primarily caused by the ascomycete fungal pathogen *Fusarium graminearum.* Infection of floral spike tissues is characterised by the biosynthesis and secretion of potent trichothecene mycotoxins, of which deoxynivalenol (DON) is widely reported due to its negative impacts on grain quality and consumer safety. The *TRI5* gene encodes an essential enzyme in the DON biosynthesis pathway and the single gene deletion mutant, *ΔTri5*, is widely reported to restrict disease progression to the inoculated spikelet. In this study, we present novel bioimaging evidence revealing that DON facilitates the traversal of the cell wall through plasmodesmata, a process essential for successful colonisation of host tissue. Chemical complementation of *ΔTri5* did not restore macro- or microscopic phenotypes, indicating that DON secretion is tightly regulated both spatially and temporally. A comparative qualitative and quantitative morphological cellular analysis revealed infections had no impact on plant cell wall thickness. Immuno-labelling of callose at plasmodesmata during infection indicates that DON can increase deposits when applied exogenously, but is reduced when *F. graminearum* hyphae are present. This study highlights the complexity of the inter-connected roles of mycotoxin production, cell wall architecture and plasmodesmata in this highly specialised interaction.

42 # Introduction

43 *Fusarium graminearum* (teleomorph *Gibberella zeae*) is an ascomycete fungal pathogen and the main
44 causative agent of Fusarium Head Blight (FHB), or scab disease, on wheat. *F. graminearum* infects
45 wheat floral tissues at flowering (anthesis), secreting many cell wall-degrading enzymes (CWDEs),
46 other proteins and metabolites as well as mycotoxins that contaminate the developing grain,
47 rendering it unsuitable for both human and livestock consumption (McMullen et al., 2012). Among
48 these mycotoxins, the sesquiterpenoid type B toxins of the trichothecene class are particularly potent
49 and include deoxynivalenol (DON), nivalenol (NIV), zearalenone (ZEA), and T-2 toxin (reviewed
50 McCormick et al., 2011), all of which target the ribosome and inhibit protein synthesis (Brown et al.,
51 2004). Trichothecene contamination of grain causes significant economic losses annually (McMullen
52 et al., 1997), destroying wheat crops weeks before harvest and subsequently proliferating during
53 ineffective grain storage/shipment. Epidemics of FHB occur when warm, wet weather coincides with
54 anthesis and are particularly prominent in the mid-West USA, Asia, Brazil and Northern Europe
55 (McMullen et al., 1997; Vaughan, Blackhouse and Del Ponte, 2016). Novel genetic targets are required
56 to help control outbreaks of FHB disease due to the prevalence of resistance to the major class of
57 azole fungicides in global *F. graminearum* strains (Fan et al., 2013). Incidences of FHB outbreaks are
58 expected to increase as climate change increases precipitation around wheat harvests (Vaughan,
59 Backhouse and Ponte, 2016). Hence, it is imperative that the infection biology of *F. graminearum* is
60 explored further to aid in the development of resistant wheat varieties and precise chemical control,
61 with the overall aim of minimising FHB-associated reductions in cereal yields, grain quality and to
62 improve human/animal health.

63 The infection cycle of FHB commences with the dispersal of conidia (asexual) or ascospores
64 (sexual) by rain droplet-induced splashes or wind onto wheat plants. During a typical infection of
65 wheat at crop anthesis, germinating spores enter the host floral tissues through natural openings,
66 such as stomata (Pritsch et al., 2000) and cracked open anther sacs, or have been reported to form

67 penetration pegs on the abaxial surface of the palea and lemma tissues of the wheat spikelet (Wanjiru,
68 Zhensheng and Buchenauer, 2002). Host-tissue colonisation continues with the invasive hyphae
69 growing both intercellularly and intracellularly. *F. graminearum* has been noted to have a 'biphasic'
70 lifestyle, whereby the advancing infection front is split between macroscopically symptomatic and
71 symptomless phases (Brown et al., 2011). The symptomless phase is hallmarked by apoplastic growth,
72 and the symptomatic by extensive intracellular growth. What initiates this switch is not yet known and
73 is a subject of great interest. During later stages of infection, *F. graminearum* secretes CWDEs in
74 abundance (Brown, Antoniw, and Hammond-Kosack, 2012) to facilitate infection by deconstructing
75 wheat cell walls. At the rachis internode, invasive hyphae have been reported to enter vascular
76 elements (Wanjiru et al., 2002) and grow through the remaining wheat spike within the vasculature
77 as well as in the cortical tissue surrounding the vascular bundles (Brown et al., 2010). Furthermore,
78 within the chlorenchyma band of the rachis, *F. graminearum* produces perithecia, sexual reproductive
79 structures, completing its lifecycle (Guenther and Trail, 2005). Post-harvest, *F. graminearum*
80 overwinters saprophytically on crop debris or within the soil, thereby infecting subsequent crop cycles.
81 The presence of *F. graminearum* in the soil can be the primary cause of seedling blight and root rot in
82 subsequent wheat crops (Parry et al., 1995).

83 Intracellular growth by *F. graminearum* has been previously reported to traverse wheat cell
84 walls though pits, or pit fields, where plasmodesmata are present (Guenther and Trail, 2005; Jansen
85 et al., 2005; Brown et al., 2010). PD are cytoplasmic communication channels that symplastically
86 bridge the cell walls by an appressed endoplasmic reticulum (ER), known as a desmotubule, within a
87 plasma membrane (PM) continuum stabilised by proteins connected to both the ER and PM (Sager
88 and Lee, 2018). PD are instrumental to cellular signalling, allowing for the transport of sugars, ions and
89 small proteins, to name a few. However, plants can adjust the permeability of PD by the deposition of
90 callose, mediated by the action of callose synthases and β-1,3-glucanases (Lee and Lu, 2011) at PD
91 junctions. This callose plugging leads to the symplastic isolation of cells that are damaged or under
92 pathogen attack thereby restricting the movement of secreted pathogen effector proteins, toxins and

93 other metabolites. PD have a major role in host plant defence against viruses, bacteria and fungi (Lee
94 and Lu, 2011). *F. graminearum* exploits the plasmodesmatal transit highways by excreting β-1,3-
95 glucanases: enzymes that catalyse the breakdown of the 1,3-O-glycosidic bond between glucose
96 molecules in callose. RNA-seq analysis of *F. graminearum* infection of wheat spikes found that several
97 Fusarium β-1,3-glucanases are upregulated in the host plant from as early as 6 hours post-infection
98 and peaking between 36-48 hours after inoculation (Pritsch et al., 2007).

99 The trichothecene mycotoxin DON is a well-reported virulence factor in wheat floral tissues
100 (Proctor et al., 1995; Jansen et al., 2005, Cuzick, Urban and Hammond-Kosack, 2008) and biosynthesis
101 of the toxin requires the *TRI5* gene, encoding the enzyme trichothecene synthase (Hohn et al., 1993).
102 DON is synthesised and then secreted by *F. graminearum* hyphae during infection and is a potent
103 ribosomal-binding translational inhibitor. This broad-spectrum dampening of induced protein
104 dependent defence responses has thus far prevented the elucidation of specific components of host
105 immunity that restrict *F. graminearum* in the DON-deficient interaction. The low molecular weight of
106 trichothecenes and their water-solubility allow them to rapidly enter cells and target eukaryotic
107 ribosomes. This causes what is known as the 'ribotoxic stress response' that can activate, among other
108 processes, mitogen-activated protein kinases (MAPKs) and apoptosis (reviewed Pestka, 2008).
109 Deletion of *TRI5* eliminates the ability of *F. graminearum* to synthesise DON (Proctor et al., 1995), and
110 infection of wheat floral tissues by the single gene deletion mutant (*ΔTri5*) is restricted to the
111 inoculated spikelet, and results in the production of eye-shaped lesions on the outer glume (Jansen et
112 al., 2005; Cuzick, Urban and Hammond-Kosack, 2008). Conversely, expression of *TRI5* in wild-type *F.*
113 *graminearum* is correlated with DON accumulation *in planta* (Hallen-Adams et al., 2011). In non-host
114 pathosystems, such as the model plant species *Arabidopsis thaliana*, infection of floral tissues with
115 the single gene deletion mutant *ΔTri5* causes a wild-type disease phenotype, indicating that DON is
116 not a virulence factor in this interaction (Cuzick, Urban and Hammond-Kosack, 2008). Current
117 evidence indicates that the *TRI4* gene, which encodes a multi-functional cytochrome P450
118 monooxygenase and resides within the main trichothecene mycotoxin biosynthetic cluster (Tokai et

119 al., 2007), is expressed during the *F. graminearum*-wheat coleoptile interaction (Qui et al., 2019), but
120 the role of *TRI4* or *TRI5* as a virulence factors in coleoptiles has not yet been reported. The TRI4 protein
121 is required for four consecutive oxygenation steps in trichothecene mycotoxin biosynthesis (Tokai et
122 al., 2007), thus indicating a role for trichothecene mycotoxins during coleoptile infection. Through the
123 use of fluorescent marker reporter strains, the *TRI5* gene has been shown to be induced during
124 infection structure formation on wheat palea (Boenisch and Schäfer, 2011). However, the absence of
125 *TRI5* in a *F. graminearum ΔTri5-GFP* strain did not impact the ability of *F. graminearum* to form
126 infection cushions during initial time points of infection (Boenisch and Schäfer, 2011). The DON
127 mycotoxin naturally occurs as two chemotypes, 15-ADON and 3-ADON, and individual *F. graminearum*
128 strains secrete either toxin type. The wild-type (WT) strain used in this study, PH-1, synthesises 15-
129 ADON. Host-plant resistance to DON is a characteristic of type II FHB resistance, whereby fungal
130 advancement does not proceed beyond the rachis node (reviewed Mesterházy, 1995).

131 Whilst the macro-biology and some aspects of the cellular biology of the single-gene deletion
132 mutant *ΔTri5* have been previously studied, the mode of restriction of *ΔTri5* remains to be elucidated.
133 Postulations have been made around the role of DON during host-tissue colonisation, specifically
134 relating to the targeting of ribosomes and the subsequent, broad-spectrum, protein translation
135 inhibition (Pestka, 2010). However, what host defence mechanisms are targeted/specifically affected
136 by DON have not been explored *in planta*. This study aims to re-evaluate the infection biology of the
137 *ΔTri5* strain, and hence the role(s) of DON, during host-tissue colonisation through a combination of
138 molecular and microscopy techniques. Through qualitative and quantitative image analysis of wheat
139 floral tissues during WT and *ΔTri5* infection, we report that the *ΔTri5* single gene deletion mutant has
140 an impaired ability to traverse plasmodesmata. We also find no evidence to support the hypothesis
141 that a general increase in plant cell wall thickening occurs in the absence of DON production, whereby
142 the upregulation of cell wall defences occurs during pathogen attack. From the data gathered, we infer
143 that the secretion of DON during host-tissue colonisation is highly specific both spatially and
144 temporally. This is indicated by the lack of increase in virulence in the *ΔTri5* mutant when supplied

145 with DON at the point of inoculation in our study. In light of these discoveries, we pose new questions
146 surrounding *F. graminearum* infection biology, cell wall colonisation and wheat host defence
147 mechanisms.

148 # Results

149 The role(s) of DON during *F. graminearum* infection of different wheat tissues was addressed through
150 a multifaceted approach. We applied a combination of detailed cell and molecular biology and
151 morphological analyses of floral and coleoptile infections to analyse the effect of DON on hyphae
152 traversing cell walls at PD and the occurrence of the defence response, callose deposition, at
153 plasmodesmata during infections cause by either the wildtype (WT) strain or the single gene deletion
154 mutant *ΔTri5 F. graminearum* strain.

155 **DON is not required for virulence on wheat coleoptiles and chemical complementation does not**
156 **restore the WT disease phenotype on wheat spikes**

157 To determine whether DON is or is not required for virulence on wheat coleoptiles under our
158 conditions the fully susceptible cv. Apogee was tested. Inoculation of wheat coleoptiles revealed no
159 differences in lesion length between the WT PH-1 strain and single gene deletion mutant *ΔTri5* (Fig. 1
160 (a) and 1(b)). However, RT-qPCR analysis showed that the WT strain expressed TRI5 during coleoptile
161 infection at 3, S5 and 7 days post inoculation (dpi), but remains at very low levels (x0.8 FgActin) and
162 stationary throughout the infection progression (Fig. 1(c)), indicating that TRI5 mRNA levels are not
163 temporally altered for this interaction during the early to mid-time points explored. This finding
164 supports a previous study by Qui et al. (2019), who reported accumulation of transcripts of the *TRI4*
165 gene, also required for trichothecene mycotoxin biosynthesis.

166 Next, we asked whether the same host and pathogen genotypes showed different DON dependencies
167 during floral tissue interactions. Disease progression of WT, *ΔTri5* and DON-complemented strains

168 were analysed by tracking visible disease symptom development on the outer glume and rachis of
169 inoculated wheat spikes. The single *ΔTri5* mutant was restricted to the inoculated spikelet in all
170 instances. Whereas chemical complementation of the *ΔTri5* mutant with DON (35ppm) applied along
171 with the conidia failed to restore the macroscopic WT spikelet phenotype occurring on the inoculated
172 spikelet or spikelet-to-spikelet symptom development. This DON concentration was not detrimental
173 to either spore germination or early spore germling growth (supplementary S1). Interestingly, co-
174 inoculation of WT *F. graminearum* with DON at the same concentration did not result in any
175 observable advancement of disease symptoms (Fig. 2 (a)). Application of DON (35ppm) alone did not
176 induce any macroscopic disease symptoms and visually equated to the water only (dH_2O) mock-
177 inoculated samples (Fig. 2 (d), 3(a)). The area under the disease progression curve (AUDPC) analysis
178 revealed that the PH-1 and PH-1 + DON supplementation floral infections had significantly greater
179 disease progression than the *ΔTri5*, *ΔTri5* + DON, DON only, and mock-inoculated treatments (Kruskal-
180 Wallis, $p=2.8e^{-10}$; Fig. 2 (b)). To quantify the levels of DON present in all treatments at the end of
181 disease progression (day 14), a DON-ELISA test was carried out to determine the final 15-ADON
182 concentrations. PH-1 and PH-1 + DON samples had an average DON concentration of over 30 ppm,
183 whilst all other treatments had no detectable (<0.5ppm) DON (Fig. 2 (c)). This indicates that the
184 addition of DON to WT inoculum did not stimulate further DON production and confirms that the PH-
185 1 *ΔTri5* mutant is impaired in DON biosynthesis. Of note, the lack of detection of DON in the *ΔTri5* +
186 DON and DON alone samples is likely due to the detoxification of DON by wheat plants to DON-3-
187 glucoside, the latter is undetectable by the competitive enzyme-labelled immunoassay kit used in this
188 study. The conjugation of DON to DON-3-glucoside, catalysed by a UDP-glucosyltransferase, *in planta*
189 is difficult to detect through its increased molecule polarity and is thus known as a 'masked mycotoxin'
190 (Berthiller et al., 2005). A visual representation of disease progression occurring in each treatment is
191 shown in Fig. 2 (d).

192 Cuzick, Urban and Hammond-Kosack (2008) had previously shown that a qualitative difference in the
193 appearance of macroscopic disease symptoms on the glumes between the WT and the *ΔTri5* mutant.

194 In this study, we have extended this observation and explored the macroscopic as well as the
195 microscopic disease symptoms. Macroscopically, we were able to confirm the *ΔTri5*-inoculated
196 spikelets exhibited 'eye-shaped' lesions on the outer surface of the glume by 7dpi (Fig. 3 (a)). These
197 differed from the characteristic fawn brown 'bleaching' of the spikelet tissues observed in the WT
198 interaction at 7dpi (Fig. 3 (a)). Chemical complementation of *ΔTri5* did not restore the WT phenotype
199 nor visibly increase the severity of the WT disease phenotype. To quantify the diseased area,
200 inoculated spikelets were imaged at 5 and 7dpi and analysed using the Lemnagrid software for
201 diseased area. The PH-1 and PH-1 + DON spikelets had a greater area exhibiting disease symptoms
202 than both the *ΔTri5* and *ΔTri5* + DON treatments (Fig. 3 (b)). N. B. Computational restrictions in spikelet
203 parsing from background led to minor, insignificant disease symptoms for DON and mock samples.

204 **The *ΔTri5* mutant is inhibited in its ability to traverse plasmodesmata during host-tissue colonisation**

205 Resin-embedded samples of the lemma, palea and rachis spikelet components revealed changes in
206 cellular morphology at different points of infection (Fig. 4). In the palea and lemma parenchyma tissue
207 layer, the *ΔTri5* and *ΔTri5* + DON infected samples exhibited extensive cell wall degradation and
208 colonisation by invasive hyphae (Fig. 5), similarly to the WT infection. However, in the adaxial layer of
209 the palea and lemma tissues, the hyphae in the *ΔTri5* and *ΔTri5* + DON samples rarely penetrated into
210 the thicker-walled cells (Fig. 5(a)-(d)). Mirroring the macroscopic lack of symptoms in the rachis, the
211 *ΔTri5* rachis samples never contained invasive hyphae at either 5 or 7 dpi (Fig. 5(e)). In the PH-1 and
212 PH-1 + DON infected samples, invasive hyphae proliferated throughout the entirety of the lemma,
213 palea and rachis tissues, causing extensive cell wall degradation (Fig. 4). To penetrate the adaxial layer,
214 the PH-1 hyphae utilised cell wall pits resembling PD pit fields (Fig. 4(c)). In these instances, the hyphae
215 constricted considerably to traverse the cell wall. Traversing of the cell wall through PD pit fields was
216 not observed in *ΔTri5* and *ΔTri5* + DON samples at either time point (Fig. 5). In general, where hyphae
217 had invaded cells, the cell contents, notably nuclei, chloroplasts and evidence of cytoplasm, were not
218 observed, indicating cell death. In the palea and lemma tissues of the PH-1 infected samples at 7dpi,

219 putative evidence of 'ghost' hyphae was identified, which are characterised by a lack of cellular
220 contents (Brown et al., 2011) in older infection structures as the infection front advances into the host
221 plant.

222 To aid elucidation of the role of DON during infection of wheat floral tissues, cell wall thickness from
223 resin-embedded wheat samples was measured along the adaxial layer of lemma and palea tissues,
224 and in the visibly reinforced regions of rachis tissue, for all treatments. In the adaxial layer of the
225 lemma, palea and rachis tissues, cell wall thickness was found not to differ between treatments,
226 particularly between those with and without the presence of DON (Supplementary file S5). This
227 unanticipated result indicates that cell wall reinforcements are not evident at this level of resolution,
228 and are not impacted by the presence of DON. However, it is worth noting that extensive cell wall
229 degradation was present in the abaxial layer of palea and lemma tissues. This microscopic phenotype
230 was not quantified but is most likely caused by the release of CWDEs from *F. graminearum* hyphae
231 (Supplementary file S5).

232 In order to gain a thorough understanding of infection, a scanning electron microscopy analysis was
233 used. SEM micrographs of rachis post spikelet inoculation with WT PH-1 at 5dpi revealed several
234 notable interactions, including intracellular growth through cells still containing cytoplasm, apoplastic
235 growth between cells, hyphal constriction and cell wall traversing and gaps in rachis cell walls (Fig.
236 6(a), (b) and (d)). Micrographs of *ΔTri5*-infected lemma tissue at 5dpi confirmed the resin analysis,
237 whereby extensive cell wall degradation was observed in the parenchyma tissue layer (Fig. 6(c)).

238 **Immuno-labelling of callose during infection reveals reduced deposits in the WT infection and**
239 **phloroglucinol staining indicates lignin-based defence response(s)**

240 Resin sections of PH-1, *ΔTri5* and mock-inoculated wheat floral tissues were analysed for the presence
241 of callose at junctions in the cell wall (Fig. 7). Immuno-labelling for the presence of callose confirmed
242 the material of pit structures was consistent with plasmodesmata. Imaging revealed that in both WT
243 (PH-1) and DON-deficient (*ΔTri5*) *F. graminearum*-inoculated spikes there was an increased frequency

244 of instances where callose was deposited at plasmodesmatal junctions compared to mock-inoculated
245 controls (Fig. 7). However, the DON only inoculated samples exhibited a marked increase in callose in
246 both lemma and rachis tissues, indicating that callose deposition had been induced in a manner
247 consistent with a basal immune response to symplastically isolate cells after the detection of the DON
248 toxin.

249 Spikelets of wheat inoculated with WT, PH-1 and *ΔTri5* were sampled at 5dpi for analysis of
250 the lignin response. This investigation was prompted by the presence of localised 'eye-shaped' lesions
251 in the *ΔTri5*-infected samples. Darker staining by the phloroglucinol indicates a higher lignin content,
252 which was found to be most notable in the *ΔTri5*-infected lemma tissue (Supplementary file S8). This
253 was surprising, as the lesions were present on the glume. Whilst this was not quantified, the WT PH-
254 1 and mock-inoculated controls were visually comparable, indicating that WT *F. graminearum* may
255 have a role in dampening pathogen-induced lignin upregulations, possibly through the action of DON.
256 This proposes the hypotheses that in the absence of trichothecene mycotoxins, wheat is able to
257 upregulate lignin defence pathways.

258 Discussion

259 This study has re-examined and extended knowledge on the restricted host tissue colonisation
260 phenotype previously reported in wheat spikes for the non-DON-producing *ΔTri5* single gene deletion
261 mutant of *F. graminearum*. The study was catalysed by the lack of published cellular information
262 available on how DON, produced and secreted by the advancing *F. graminearum* hyphae, actually
263 facilitates the extraordinary effective and speedy disease progression consistently observed in the
264 spikes of susceptible wheat cultivars. DON has long been classified as a key virulence factor in the *F.*
265 *graminearum*-wheat interaction (Hohn et al., 1993; Jansen et al., 2005) and facilitates the host-tissue
266 colonisation of the rachis and thus is essential for successful internal spikelet-to-spikelet growth of
267 hyphae through the entire floral spike. However, prior to this study, the morphological and cellular

268 responses underlying this macroscopically well documented phenomenon had not been explored. In
269 this study our two primary aims were (a) to identify the morphological differences in the hyphal
270 infection routes between the wild-type (WT) and *ΔTri5* strains during wheat floral infections compared
271 to coleoptile infections, and (b) to focus on the multifaceted role(s) of the cell wall and its constituent
272 components as well as the pit fields during hyphal colonisation due to their potential to delay,
273 minimise or cease fungal progression through the numerous internal complexities that the wheat
274 spike architecture presents to the *Fusarium* hyphae.

275 As described above, our experimentation confirmed that the *ΔTri5* mutant could sufficiently
276 colonise the lemma and palea tissues but not the rachis (Jansen et al., 2005; Cuzick et al., 2007).
277 Similarly, our results concurred with those of Jansen et al. (2005) that the DON-deficient *F.*
278 *graminearum* strain could not grow beyond the rachis node due to the presence of inherently thicker
279 cell walls in this tissue. However, our quantitative comparative analysis of the WT and DON-deficient
280 interactions revealed no differences between cell wall thickness at two timepoints, or with the control
281 mock inoculated tissues, indicating that cell walls do not increase in thickness *per se* as part of a locally
282 occurring defence response. Upon further microscopic analysis in the current study, we observed that
283 the DON-deficient *ΔTri5* mutant could not enter wheat cells with inherently thicker cell walls because
284 the hyphae could not pass through pit fields containing plasmodesmata. This phenomenon was
285 frequently observed in both the cortical and sclerenchyma cell layers. As a result, the *ΔTri5* hyphae
286 accumulated within and between the neighbouring thinner-walled parenchyma cells. In the absence
287 of DON, potentially other so far uncharacterised secreted proteinaceous effectors fail to correctly
288 manipulate these potential gateways into the neighbouring wheat cells. The analysis of resin sections
289 revealed that cell walls within the adaxial layer of lemma and palea tissues were not thicker in infected
290 samples. Although this rules out additional cell wall reinforcements, these findings do not eliminate
291 cell wall compositional changes. Our results indicate that lignin content increases in the lemma tissue,
292 which strengthens the tissue and hence emphasises the role of plasmodesmata as cell wall portals in
293 host-tissue colonisation. We hypothesise that DON, through its intracellular target of the ribosomes,

294 inhibits local protein-translation based defence responses.. Whereas symplastic isolation of
295 neighbouring cells by the deposition of callose at plasmodesmata is a largely post-translationally
296 regulated process induced within the generic plant defence response (Wu et al., 2018). Our SEM
297 inquiry of the infected tissues indicates that plasmodesmata, when used by the advancing hyphal
298 front, are potentially 'dead portals', that lack the desmotubule symplastic bridge between
299 neighbouring cells. Whether callose deposits are eliminated prior to or coincident with hyphal
300 constriction and traversing of the cell wall will require the use of another microscopy technique,
301 namely TEM. Although again a static analysis method, TEM can be used to explore whether
302 desmotubule connections, and callose deposits, are consistently present or absent at the point of
303 hyphal traverse. Collectively, these data suggest that the broad-spectrum consequences of DON
304 targeting could prevent the synthesis and action of key defence enzymes at plasmodesmata. This
305 could be explored by a combined comparative proteomics, phosphoproteomics and RNAseq analysis
306 of the WT and *ΔTri5*-infections to elucidate the wheat defence responses occurring at the advancing
307 *Fusarium* hyphal front that are reduced and/or eliminated by the presence of DON.

308 The deposition of callose at the plasmodesmatal junction by callose synthases has been
309 demonstrated to be induced by various biotic stress-inducing pathogens (Wu et al., 2018). The role of
310 callose differs with cellular location: callose polymers are a structural component of papillae in various
311 cereal species that form below appressoria produced by fungal pathogens such as the powdery
312 mildew *Blumeria graminis* f. sp. *hordei*, whereby elevated callose deposition in highly localised papillae
313 in epidermal cells result in resistance to fungal infection (Ellinger et al., 2013). In vascular tissue, callose
314 can be deposited to restrict vascular advancements by wilt pathogens, including by *Fusarium* and
315 *Verticillium* species (reviewed: Kashyap et al., 2021). To investigate the potential of DON impacting
316 upon plasmodesmatal occlusion following our discovery of the impeded traversal of plasmodesmata
317 by the *ΔTri5* strain, we immuno-labelled callose in resin-embedded sections of wheat floral tissues.
318 We found that DON strongly induced callose depositions, and callose deposition was also moderately
319 increased in WT and *ΔTri5* infected lemma and palea tissues. This indicates that callose deposition is

320 increased as a defence response when DON or *Fusarium* hyphae are present. However, in the WT
321 infection, we observed a frequency of callose depositions similar to the non-DON producing *ΔTri5*
322 strain indicating an interruption or targeted degradation of callose occlusions by *F. graminearum*
323 invasive hyphae. The secretion of glycoside hydrolase (GH) proteins that break down β-1,3-glucans
324 such as callose have not been explored with respect to the *Fg*-wheat interaction, although GH12 family
325 proteins that break down xyloglucan in plant cell walls appear to be implicated in virulence (Wang et
326 al., 2022). In the *ΔTri5* infections, in the absence of DON other hyphal components and /or secreted
327 molecules may be responsible for the modest callose deposition at the plasmodesmatal junction.

328 Intracellular colonisation through the rachis node and beyond in the rachis internode possibly
329 requires DON and is therefore required for the second intracellular phase of the biphasic lifestyle
330 described for *F. graminearum,* where extracellular apoplastic growth characterises the initial 'stealth'
331 phase of infection (Brown et al., 2010). If this is the case, then lacking the ability to traverse
332 plasmodesmata would restrict direct acquisition of nutrients from host cells by the fungal hyphae. The
333 *TRI* biosynthetic gene cluster required for DON biosynthesis is transcriptionally activated early during
334 wheat spike infection, peaking between 72 and 120 hrs post-inoculation (Evans, 2000; Cheng, Kistler
335 and Ma, 2019), when infection is largely restricted to the palea, lemma and glume tissues.
336 Trichothecene biosynthesis is regulated by two transcription factors, TRI6 and TRI10, within the
337 biosynthetic pathway. Of note, DON is not required for full virulence of the developing wheat kernel
338 seed coat (Jansen et al., 2005), in addition to our finding in coleoptiles, Ilgen et al. (2009) identified
339 that trichothecene biosynthesis pathway induction was potentially tissue specific and somewhat
340 restricted to the developing grain kernel and rachis node, and suggested that 'kernel tissue
341 perception' by the *Fusarium* hyphae induce the biosynthesis of trichothecene mycotoxins. This
342 suggestion concurs with Zhang et al. (2012) who report that the trichothecene biosynthesis genes
343 were not induced during *F. graminearum* infection of wheat coleoptiles, whereas Qui et al. (2019)
344 reported the expression of *TRI4* in wheat coleoptiles. We found *TRI5* expression to be detectable at
345 low levels in the wheat coleoptiles, remaining around 0.8 x the expression levels of FgActin. This is

346 lower than the TRI5 expression level reported by Brown et al. (2011), who reported a level over 3 x
347 that of FgActin in wheat spikes.

348 Gardiner et al. (2009b) presented evidence that, in addition to their previous reports that
349 exogenous application of amines, such as agmatine, *in vitro* induces *TRI5* expression (Gardiner et al.,
350 2009a), low pH further accelerates expression of the *TRI* gene cluster. Other inducers of the DON
351 biosynthetic pathway genes include carbon, nitrogen and light (Gardiner et al., 2009b). These factors
352 could explain the low and stationary levels of *TRI5* gene expression throughout infection of wheat
353 coleoptiles, which have been noted to be particularly acidic plant tissue due to the optimum activity
354 of expansion proteins around pH 4 (Gao et al., 2008). Other fungal pathogens that are reported to
355 utilise plasmodesmata during infection of cereals include *Magnaporthe orzyae* and *M. oryzae*
356 pathotype *triticum* which respectively cause rice blast and wheat blast diseases on the floral panicles
357 and floral spikes (Sakulukoo et al., 2018, Fernandez and Orth, 2018). Although *Magnaporthe oryzae*
358 does not synthesise trichothecene mycotoxins, the invading hyphae secrete another potent general
359 protein translation inhibitor, namely tenuazonic acid (Wilson and Talbot, 2009). The effect of this
360 mycotoxin on plasmodesmatal traversing and virulence in *Magnaporthe spp*. has not yet been
361 reported.

362 *F. graminearum* progression into the rachis and through sequential rachis nodes and
363 internodes allows for the successful completion of the disease infection cycle in wheat crops. Typically,
364 perithecia form from the chlorenchyma band of the rachis following prolific hyphal colonisation of this
365 highly specialised photosynthetic tissue layer within the wheat spike (Guenther and Trail, 2005).
366 Hence, interruption of WT disease progression prior to this crucial point in the primarily monocyclic
367 infection cycle is of great interest for reducing full virulence of FHB and in particular in reducing the
368 abundance of air dispersed ascospores. Interestingly, infection of barley spikelets with WT *F.*
369 *graminearum* is solely restricted to the inoculated spikelet, similarly to *ΔTri5* infection of wheat

370 (Jansen et al., 2005). How this occurs has not yet been explored, but we hypothesise that a lack of
371 traversing of plasmodesmata by hyphae may have a role to play in barley rachis node tissue.

372 Overall, our study indicates that plasmodesmata are the key to successful host-tissue
373 colonisation by *F. graminearum* and that DON, directly or indirectly, facilitates this interaction. We
374 anticipate that the results of this study are considered in future working disease models of the *F.*
375 *graminearum* - wheat interaction and suggest these incorporate a greater emphasis on tissue and cell
376 wall architecture and composition when considering host susceptibility to fungal pathogens. To this
377 end, we have proposed a new working model (Fig. 8), that summarises our findings around the
378 presence of DON during wheat infection and the impact on callose deposition at plasmodesmata.

379 Experimental Procedures

380 **Fungal growth**

381 The *Fusarium graminearum* reference strain PH-1 (NCBI: txid229533) and the DON-deficient single
382 gene deletion mutant *ΔTri5*, within the PH-1 parental background (Cuzick et al., 2008), were used in
383 this study. Conidia for glycerol stocks were prepared by culturing on Synthetic Nutrient Poor Agar
384 (SNA) plates containing 0.1% KH_2PO_4, 0.1% KNO_3, 0.1% $MgSO_4 \cdot 7H_2O$, 0.05% KCl, 0.02% glucose, 0.02%
385 sucrose and 2% agar. Plates were left to grow for 8 days at room temperature (RT) with constant
386 illumination under near-UV light (Philips TLD 36W/08). TB3 liquid medium (0.3% yeast extract, 0.3%
387 Bacto Peptone and 20% sucrose) was added to plates to stimulate spore production and left for a
388 further 2 days. Conidia were harvested and stored in 15% glycerol at -80°C in 2ml cryotubes (Thermo
389 Fisher Scientific, MA, USA). Conidial suspensions in water to be used for inoculations were prepared
390 by spreading conidia from glycerol stocks onto Potato Dextrose Agar (PDA, Sigma Aldrich, UK) plates,
391 then growth at RT for 2 days, harvesting with dH_2O and spore concentrations measured with the aid
392 of a haemocytometer (Hausser Bright-line, USA). Experiments were conducted under APHA plant
393 licence number 101948/198285/6.

394 **Plant growth**

395 The susceptible dwarf spring wheat (*Triticum aestivum*) cultivar (cv.) Apogee was used for all wheat
396 experiments, sourced from the National Small Grains Collection, USDA-ARS, Aberdeen, Idaho, USA.
397 Seeds were sown in Rothamsted Prescription Mix (RPM) soil (Petersfield Growing Mediums, UK) in
398 P15 pots (approx. volume 7cm^3) and grown in controlled environment facilities at HSE category 2
399 (Fitotron®, Weiss Gallenkamp, UK), 16hr light: 8hr dark cycle at 22°C and 18°C respectively, 70%
400 relative humidity and illumination at 2.2x10^3 µmol m^{-3}.

401 **Coleoptile inoculations**

402 For coleoptile inoculations, Apogee grain were left for 2 days at 5°C in water for imbibition before
403 being placed individually onto cotton wool plugs in a 24-well tissue culture plate (VWR, USA) and left
404 to germinate for 3 days under high humidity conditions (<90% relative humidity) under normal wheat
405 growth conditions. At 3 days post-sowing, approximately 5mm from the tip of each coleoptile was cut
406 to encourage infection. Inoculations occurred through the placement of a cut pipette tip with a filter
407 paper insert soaked with 5x10^5 spores/ml solution, with dH_2O used as a negative control. The
408 coleoptiles were left in the dark for 3 days to aid infection, after which inoculation tips were
409 subsequently removed, and coleoptiles were left to grow under normal growth conditions for a further
410 4 days (Darino et al., 2024). Disease phenotypes on the coleoptiles were assessed at 7 days post
411 inoculation by imaging lesions on a Leica M205 FA Stereomicroscope (Leica Microsystems, UK). Each
412 experimental replicate contained 5 biological samples for each treatment (3 mock-inoculated) and the
413 experiment was repeated 3 times.

414 **Floral inoculations**

415 At mid-anthesis, wheat plants were inoculated with 5 x10^5 spores/ml water conidial suspension of PH-
416 1 or *ΔTri5*, conidial suspension supplemented with DON, DON alone or water (dH_2O) control. DON
417 supplementation of inoculum was 35ppm (Sigma-Aldrich, USA). As described in Lemmens et al. (2005),

418 a 5µl droplet was placed between the palea and the lemma on each side of the 7th true spikelet from
419 the base. Inoculated plants were placed in a high (<90%) humidity for the first 72 hours of infection,
420 with the first 24 hours in darkness. After 72 hours plants were returned to normal growth conditions.

421 **Determination of DON concentration for exogenous application**

422 To determine the concentration of DON to utilise for the chemical complementation experiments, a
423 number of experiments were undertaken. These scoped for a concentration that was not detrimental
424 to both *F. graminearum* spore germination and growth (supplementary S1), as well as sufficient to
425 cause physiological stress to plant tissue (supplementary S2). Concentrations up to 350ppm were non-
426 detrimental to fungal proliferation in media and as low as 10ppm demonstrated considerable
427 reduction in growth in *Arabidopsis thaliana* seedlings. The concentration of 35ppm (118µM) was
428 determined as a result of these experiments.

429 **Disease progression**

430 As above, Apogee at mid-anthesis was inoculated and disease progression was assessed by counting
431 spikelets showing visible symptoms every 2 days after inoculation until 14 dpi. Area Under Disease
432 Progression Curve (AUDPC) (Van der Plank, 1963) values were calculated using the 'agricolae' package
433 (version 1.4.0, de Mendiburu and Yaseen, 2020) in R (version 4.0.2). Statistical significance was
434 determined by Kruskal-Wallis one-way analysis of variance through the R package 'ggplot2' (version
435 3.4.0, Wickham, 2016).

436 **Red Green Blue (RGB) colour classification for disease assessment of dissected spikelets**

437 To quantify disease progression on wheat spikelets at 5 and 7dpi, colour (RGB) spikelets were imaged
438 (iPhone 6s, Apple Inc, US) on both sides with consistent illumination. Diseased area was quantified
439 using a curated programme on the LemnaTec Lemnagrid software (CHAP, York, UK). Diseased area
440 was classified by pixel colour segmentation after application of filters to threshold from the
441 background, identify misclassified pixels and fill in gaps. Area attributed to anthers were omitted from

442 further analysis. The relative area attributed to each classification was then calculated in a custom R
443 script and all samples were normalised to the mean value of 'diseased' of the mock treatment due to
444 background parsing error.

445 **Bioimaging**

446 Inoculated spikelets were dissected from the wheat spikes for internal observations of infected floral
447 tissues. Spikelets were fixed for 24 hr in a solution of 4% paraformaldehyde, 2.5% glutaraldehyde and
448 0.05M Sorensen's phosphate buffer (NaH_2PO_4: $Na_2HPO_4 \cdot 7H_2O$, pH 7.2), in the presence of Tween 20
449 (Polyethylene glycol sorbitan monolaurate; Sigma-Aldrich) and subject to a light vacuum for 20s to
450 ensure tissue infiltration. Fixed spikelets were washed 3x with 0.05M Sorensen's phosphate buffer
451 and subsequently underwent an ethanol dehydration protocol at 10% EtOH increments, up to 100%
452 EtOH. Spikelets were dissected into component tissues and embedded with LR White resin (TAAB,
453 Reading, UK) at increasing resin ratios (1:4, 2:3, 3:2, 4:1), followed by polymerisation in the presence
454 of N_2 at 60°C for 16h. Ultra-thin 1µm resin sections were cut from resin blocks using a microtome
455 (Reichert-Jung, Ultracut), placed onto Polysine microscope slides (Agar Scientific, UK) and stained with
456 0.1% (w/v) Toluidine Blue O in 0.1M Sorensen's phosphate buffer (NaH_2PO_4: $Na_2HPO_4 \cdot 7H_2O$, pH 7.2).
457 Every 10th section was collected for a total of 10 sections per embedded block to fully explore floral
458 tissues and mounted with Permount (Fisher Scientific, UK) prior to imaging on a Zeiss Axioimager 512
459 (Zeiss, Oberkochen, Germany) at x20 magnification under brightfield illumination. The experiment
460 was repeated 3 times, with a total of 5 biological replicates for each treatment, with 2 mock samples
461 per batch. In total, 111 resin blocks were explored across a 100um in the centre of the sample, with
462 sections cut every 10µm. Image analysis was conducted in Fiji for ImageJ (version 2.3.0) and statistical
463 analysis was conducted in R (version 4.0.2).

464 For SEM exploration of floral tissues, spikelets at 5dpi were excised and coated in 50:50 OCT
465 compound (Sakura FineTek) with colloidal graphite (TAAB). SEM analysis was conducted on rachis

466 tissue infected with the WT reference strain PH-1 at 5dpi. Sample preparation occurred in a Quorum
467 Cryo low-pressure system before imaging on a JEOL LV6360 SEM at 5kV with software version 6.04.

468 Callose immuno-labelling of resin-embedded sectioned material was conducted according to Amsbury
469 and Benitez-Alfonso (2022). Briefly, callose was localised by anti-β-1,3-glucan antibodies (Biosupplies,
470 Australia) and secondarily conjugated with rabbit anti-mouse Alexa Fluor 488. Wheat cell walls were
471 counterstained with calcofluor white. Sections were imaged by confocal microscopy on a Leica SP8
472 confocal microscope, with excitation-emission spectra for AlexFluor-488 at 488nm, 510nm-530nm
473 and 405nm, 450nm-475nm for Calcofluor white. Image analysis for the quantification of callose
474 deposits per cell was conducted in Fiji (ImageJ) using maximum projections of Z stacks and channels
475 converted to binary masks. The number of cells in the sample area was calculated using the cell
476 counter tool and callose deposits were counted by the number of discrete Alexa 488-fluorescences
477 between the size of 2 to 12 pixel units to eliminate cross-reactivity with β-1,3-glucans in the fungal cell
478 walls. The number of callose deposits were averaged across the number of complete cells (all cell walls
479 visible) in the sample area. Callose deposits were quantified in the lemma and rachis tissues only, with
480 3 biological replicates for each treatment (PH-1, *ΔTri5*, DON, Mock). Further examples are present in
481 supplementary file S6 and image analysis methodology is demonstrated in supplementary S7.

482 **DON quantification**

483 To determine if the presence of DON in the WT strain inoculum stimulated further DON production, if
484 administered DON could be detected in wheat spike tissues at the end of disease progression (14dpi),
485 and the absence of DON in the *Δtri5* mutant interaction a competitive enzyme-labelled immunoassay
486 for 15-ADON was employed. Whole wheat spikes were utilised for this quantification in the case the
487 DON was trafficked or secreted beyond the inoculated spikelet due to its high water solubility. Whole
488 wheat spikes after 14 days of disease progression were ground to a fine powder in the presence of
489 liquid nitrogen and 1g of each sample was resuspended in 5ml dH_2O, vortexed until dissolved,
490 incubated in a 30°C water bath for 30 mins and centrifuged for 15 minutes at full speed (13.1g). The

491 supernatant was removed and analysed using the Beacon Analytical Systems Inc Deoxynivalenol
492 (DON) Plate Kit (Cat. 20-0016) according to kit instructions. The OD450 values were measured on a
493 Thermo Varioskan microplate reader (Thermo Scientific, USA). Three technical replicates of each
494 biological replicate (a single wheat spike) were conducted, and the experiment was repeated three
495 times.

496 **Expression of the mycotoxin biosynthesis gene TRI5 during coleoptile infection**

497 The trichodiene synthase gene *TRI5* was used as a proxy for the relative expression of the trichodiene
498 biosynthesis pathway during coleoptile infection. Total RNA was extracted from whole coleoptiles at
499 3, 5 and 7dpi using a total RNA extraction kit (NEB) and following the kit instructions. First strand cDNA
500 was synthesised using RevertAid First Strand cDNA synthesis kit (ThermoFisherSci) as per kit
501 instructions and utilising random hexamer primers provided. *TRI5* expression was then assessed by
502 qPCR with melt curve using the primers in supplementary S3, with SYBR as the reporter, passive
503 reference as ROX and NFQ-MGB as the quencher. The qPCR with melt curve was conducted in
504 technical and biological triplicate on a QuantStudio™ 6 Pro and results analysed on the complementary
505 Design & Analysis Software v. 2.6.0 (ThermoFisher Scientific, MA, USA). The experiment was
506 conducted 3 times. Quantification of *TRI5* expression was normalised against the housekeeping gene
507 FgActin (primers in supplementary S3) for each sample, also included within the qPCR run in triplicate.
508 At least one primer in a primer pair for qPCR targets was designed to span an exon-exon junction to
509 avoid annealing to residual DNA.

510 **Phloroglucinol staining for presence of lignin**

511 A 3% Phloroglucinol (Sigma Aldrich, UK) - HCl solution (Weisner stain) was prepared fresh in
512 accordance with methods by Mitra and Loqué (2014). Inoculated wheat spikelets were sampled at
513 5dpi and cleared in 100% EtOH for 4 days before going through a rehydration series (75%, 50%, 25%
514 and 0% EtOH) at 1 hour per stage. Cleared spikelets were bathed in Weisner stain for 1 hour, or until
515 staining of the tissues becomes evidently saturated. Spikelets were then imaged (OM-D E-M10,

516 Olympus, Japan) under constant illumination and, subsequently, dissected tissues were imaged
517 individually.

518 **Formation of perithecia *in vitro***

519 Carrot agar was prepared using the method outlined by Cavinder et al. (2012) and supplemented with
520 DON at 35ppm (w/v) to test for the ability of the WT strain, and the DON trichothecene-deficient
521 deletion mutant, *ΔTri5*, to develop perithecia *in vitro*, for lifecycle completion viability (Supplementary
522 S4). Ability of perithecia to discharge ascospores in the presence of DON was assessed using the same
523 method as described in Cavinder et al. (2012).

524 **Statistical analysis**

525 Scripts were written in R (version 4.0.2) for each experimental analysis. Unless otherwise stated,
526 ANOVA followed by Tukey post-hoc test was conducted for parametric datasets and Kruskal-Wallis for
527 non-parametric datasets. The significance threshold was set to $P < 0.05$ in all cases.

528

529 # Acknowledgements

530 The authors would like to thank the CHAP organisation at Rothamsted Research for access to their
531 Lemnagrid image analysis software. Special thanks are given to Hannah Walpole and Kirstie Halsey
532 from Rothamsted Research Bioimaging department for continued training, advice and expertise. We
533 also thank Harold Bockelman, the curator of the National Small Grains Collection, USDA-ARS, for
534 providing the wheat variety used in this study. Kim Hammond-Kosack and Martin Urban are supported
535 by the Biotechnology and Biological Sciences Research Council (BBSRC) Institute Strategic Programme
536 (ISP) Grants Designing Future Wheat (BBS/E/C/000I0250) and Delivering Sustainable Wheat
537 (BB/X011003/1 and BBS/E/RH/230001B) and the BBSRC grants (BB/X012131/1 and BB/W007134/1).

538 Victoria Armer is supported by the BBSRC-funded South West Biosciences Doctoral Training
539 Partnership (BB/T008741/1).

540 Author contributions

541 VA conducted the experiments and wrote the manuscript, MU generated the *Fusarium graminearum*
542 mutant, TA provided oversight and training for image analysis, MJD and KHK provided project
543 oversight, experimental design and manuscript planning, development and revisions.

544 Additional Information

545 The authors declare no financial or non-financial competing interests.

546 Data availability

547 The research data supporting this publication are provided within this paper. Requests for materials
548 relating to this paper should be made to Kim Hammond-Kosack (kim.hammond-
549 kosack@rothamsted.ac.uk) at Rothamsted Research.
550

551 Figure Legends

552 **Figure 1. *F. graminearum* disease formation on wheat coleoptiles.** (a) Length lesion at 7dpi for PH-1,
553 the *ΔTri5* mutant and mock inoculations, Kruskal-Wallis $p < 0.005$(***). (b) Examples of disease lesion
554 phenotypes at 7dpi for PH-1, *ΔTri5* and mock inoculations from rep 2, scale bar = 20mm and (c)
555 Relative expression of *TRI5* measured using RT-qPCR at 3, 5 and 7dpi in wheat coleoptiles, normalised
556 against FgActin expression. ANOVA $F(2,22) = 0.421$, $p = 0.662$ (ns).

557 **Figure 2. Analysis of whole wheat floral tissues following point inoculations.** (a) Tracked visible
558 disease progression at 2-day intervals to 14 dpi from below the inoculated spikelet. (b) Area Under

559 Disease Progression Curve (AUDPC) for disease progression in panel (a), Kruskal-Wallis p <0.005 (***).
560 (c) DON concentrations of wheat spikes at 14 dpi, Kruskal-Wallis p <0.005 (***). (d) Representative
561 disease progression images at selected timepoints of 4, 8 and 12 days.

562 **Figure 3. Quantitative spikelet analysis for disease symptom development.** (a) Examples of dissected
563 spikelets at 5 and 7dpi, scale bar = 10mm. (b) External tissue areas exhibiting disease symptoms at 5
564 and 7dpi as determined by Lemnagrid computational software. ANOVA, P < 0.005 (***), Tukey post-
565 hoc denotes group significance.

566 **Figure 4. WT-infected wheat floral tissues at 5 and 7 dpi demonstrating aspects of typical infection.**
567 (a) Lemma at 5dpi infected with WT *F. graminearum* showing widespread hyphal colonisation
568 throughout the tissue accompanied by hyphal proliferation protruding from the abaxial layer. (b) A
569 7dpi WT-infected lemma showing further tissue degradation by cell wall degrading enzymes and
570 considerable hyphal proliferation. (c) Rachis at 5dpi infected with WT *F. graminearum* showing a
571 number of plasmodesmatal crossings by invasive hyphae, indicated by yellow arrowheads, and
572 extensive cell wall degradation of the mesophyll layer by *F. graminearum*- secreted cell wall degrading
573 enzymes. Plasmodesmata can be identified as gaps in the parenchyma layer cell walls, a number of
574 which are indicated by black arrowheads. (d) A 7dpi WT-infected rachis demonstrating durability of
575 parenchyma tissue against cell wall degrading enzymes at later infection timepoints. ab = abaxial layer,
576 ad = adaxial layer, e = epidermal layer, mes = mesophyll, p = parenchyma tissue, vb = vascular bundle.
577 Yellow arrowheads indicate plasmodesmatal crossings by invasive *F. graminearum* hyphae. Scale bar
578 = 50µm.

579 **Figure 5. Comparison of *ΔTri5*-infected and *ΔTri5* + DON infected wheat floral tissues at 5dpi and**
580 **7dpi showing the similarities and differences between tissue types in various aspects of a typical**
581 **infection.** (a) Lemma at 7dpi infected with *ΔTri5 F. graminearum* with extensive proliferation of
582 invasive hyphae throughout the abaxial layer, but rarely any penetration into the adaxial layer. (b).
583 Palea at 5dpi infected with *ΔTri5* and supplemented with 35ppm DON showing cell wall degradation

584 in the abaxial layer and evidence of external fungal hyphae. Yellow arrows indicate hyphae external
585 to the plant tissue. (c) Palea at 7dpi infected with *ΔTri5*, with similar symptoms to the lemma at the
586 earlier 5dpi time point. (d) Lemma infected with *ΔTri5* and supplemented with 35ppm DON at 7dpi
587 showing cell wall degradation of the abaxial layer. (e) A rachis section at 5dpi infected with *ΔTri5* and
588 supplemented with 35ppm DON. No evidence of hyphae or cell wall degradation throughout the
589 sample. ab = abaxial layer, ad = adaxial layer, e = epidermal layer, mes = mesophyll layer, p =
590 parenchyma tissue, vb = vascular bundle. No plasmodesmatal crossings by invasive *F. graminearum*
591 hyphae are evident. Scale bar = 50µm.

592 **Fig. 6. SEM micrographs of PH-1 and *ΔTri5*- wheat floral interactions.** (a) A hypha of the wild-type
593 PH-1 strain appears to cross through the cell wall at 5dpi in rachis tissue. Scale bar = 10µm. (b) Wild-
594 type PH-1 infecting rachis tissue at 5dpi, the numbered yellow arrowhead indicates point of interest.
595 1. Intracellular growth in a cell where cytoplasm is still present; 2., 3., and 5. Apoplastic growth
596 between cells, 4. Potential crossing of the cell wall by a hypha through a plasmodesma, and 6. 'Holes'
597 in the cell wall that are potential sites of plasmodesmata. Scale bar = 20µm. (c). *ΔTri5*-infected lemma
598 tissue at 5dpi demonstrating extensive hyphal colonisation and cell-wall degradation of the
599 parenchyma tissue layer (bottom), but minimal infection in the thicker-walled adaxial layer (top), scale
600 bar = 20µm. (d) Wild-type PH-1 infection of the rachis at 5dpi, 1. Growth of two hyphae through the
601 same apoplastic space in parallel to hyphae growing intracellularly in neighbouring cells to the left and
602 right. 2. Hypha appear to constrict to traverse the cell wall. Scale bar = 10µm.

603 **Fig. 7. Immunofluorescence detection of callose in rachis and lemma tissues.** Magnified region of
604 interest of the *Fg*-wheat interaction demonstrating callose deposits at plasmodesmata. (a) Control
605 rachis, (b) rachis below DON-inoculated spikelet, (c) PH-1 infected lemma at 5dpi, (d) *ΔTri5*-infected
606 lemma at 5dpi. Sections were imaged by confocal microscopy with excitation-emission spectra for
607 AlexFluor-488 488nm, 510nm-530nm and 405nm, 450nm-475nm for Calcofluor. Callose deposits are
608 labelled in magenta with wheat cell walls in cyan. Scale bars = 50µm. In panels (c) and (d) the Fusarium

609 hyphae also react positively to the antibody due to β-1,3-glucans in the fungal cell wall and are labelled
610 in magenta. (e) Quantification of the number of immuno-labelled callose deposits, averaged across
611 number of cells in the sample area, in lemma tissues at 5dpi, ANOVA = $p < 0.05$ (*), and (f) Rachis
612 tissues at 5dpi, ANOVA = $p < 0.05$ (*). Letters indicate significance differences between groups from
613 Tukey Post-hoc analysis following one-way ANOVA.

614 **Fig. 8. Proposed working model for the role of DON in the *F. graminearum* – wheat interaction.** (a)
615 In the wild-type (WT) interaction, DON interferes with the wheat host defence response by inhibiting
616 protein translation and reducing the ability of the host to deposit callose at plasmodesmata to restrict
617 further hyphal infection. It is currently unknown how long the desmotubule remains functional, or in
618 place. (b) In the absence of DON, *Fg*-secreted proteins are detected by the host and trigger host
619 defence responses, including the symplastic isolation of neighbouring cells by the deposition of callose
620 at plasmodesmata.

621

622 # References

623 1. Amsbury, S. and Benitez-Alfonso, Y. (2022). Chapter 10: Immunofluorescence detection of callose
624 in plant tissue sections. In: Benitez-Alfonso, Y. and Heinlein, M. (eds.): *Plasmodesmata: Methods*
625 *and Protocols*, Methods in Molecular Biology, vol. 2457. doi: 10.1007/978-1-0716-2132-5_10.
626 2. Armer, V.J., Deeks, M.J. and Hammond-Kosack, K. E. (2024). *Arabidopsis thaliana* detached leaf
627 assay for the disease assessment of *Fusarium graminearum*. *Protocols.io.* doi:
628 10.17504/protocols.io.261gedmwov47/v1.
629 3. Berthiller, F., Dall'Asta, C., Schuhmacher, R., Lemmens, M., Adam, G. and Krska, R. (2005). Masked
630 mycotoxins: determination of a deoxynivalenol glucoside in artificially and naturally contaminated
631 wheat by liquid chromatography–tandem mass spectrometry. *Journal of Agricultural and Food*
632 *Chemistry.* 53(9), 3421-3425. doi: 10.1021/jf047798g.
633 4. Boenisch, M.J. and Schafer, W. (2011). *Fusarium graminearum* forms mycotoxin producing
634 infection structures on wheat. *BMC Plant Biology.* 11: 110. doi: 10.1186/1471-2229-11-110
635 5. Brown, D. W., Dyer, R. B., McCormick, S. P., Kendra, D. F. and Plattner, R. D. (2004). Functional
636 demarcation of the *Fusarium* core trichothecene gene cluster. *Fungal Genetics and Biology.*
637 41(4), 454-462. doi: 10.1016/j.fgb.2003.12.002.
638 6. Brown, N. A., Antoniw, J., Hammon-Kosack, K. E. (2012). The Predicted Secretome of the Plant
639 Pathogenic Fungus *Fusarium graminearum*: A Refined Comparative Analysis. *PLoS ONE*, 7(4),
640 e33731. doi:10.1371/journal.pone.0033731.
641 7. Brown, N. A., Bass, C., Baldwin, T. K., Chen, H., Massot, F., Carion, P. W. C. *et al.* (2011).
642 Characterisation of the *Fusarium*-wheat floral interaction. *Journal of Pathogens*. Article ID
643 626345. doi: 10.4061/2011/626345.scholar
644 8. Brown, N. A., Urban, M., van de Meene, A. M. L., and Hammond-Kosack, K. E. (2010). The
645 infection biology of *Fusarium graminearum* defining the pathways of spikelet to spikelet
646 colonisation in wheat ears. *Fungal Biology*. 114(7): 555-571. doi: 10.1016/j.funbio.2010.04.006.

647 9. Cavinder, B., Sikhakolli, U., Fellows, K. M. and Trail, F. (2012). Sexual development and ascospore
648 discharge in *Fusarium graminearum*. *Journal Visualized Experiments.* 61, 3895. doi:
649 10.3791/3895.
650 10. Chen, Y., Kistler, H. C., and Ma, Z. (2019). *Fusarium graminearum* trichothecene mycotoxins:
651 biosynthesis, regulation, and management. *Annual Review Phytopathology.* 57, 15-39. doi:
652 10.1146/annurev-phyto-082718-100318.
653 11. Cuzick, A., Urban, M. and Hammond-Kosack, K. (2008). *Fusarium graminearum* gene deletion
654 mutants *map1* and *tri5* reveal similarities and differences in the pathogenicity requirements to
655 cause disease on Arabidopsis and wheat floral tissue. *New Phytologist*. 177(4), 990-1000. doi:
656 10.1111/j.1469-8137.2007.02333.x
657 12. Darino, M., Urban, M., Kaur, N., Machado-Wood, A., Grimwade-Mann, M., Smith, D., *et al.*
658 (2024). Identification and functional characterisation of a locus for target site integration in
659 *Fusarium graminearum. Fungal Biology and Biotechnology. 11: 2.* doi: 10.1186/s40694-024-
660 00171-8 .
661 13. Dilks, T., Halsey, K., De Vos, R. P., Hammond-Kosack, K. E. and Brown, N. A. (2019). Non-
662 canonical fungal G-protein coupled receptors promote Fusarium head blight on wheat. *PLoS*
663 *Pathogens*. 15(4): e1007666. doi: 10.1371/journal.ppat.1007666.
664 14. Ellinger, D., Naumann, M., Falter, C., Zwikowics, C., Jamrow, T., Manisseri, C. *et al*. (2013).
665 Elevated early callose deposition results in complete penetration resistance to powdery mildew
666 in Arabidopsis. *Plant Physiology.* 161(3): 1433-1444. doi: 10.1104/pp.112.211011
667 15. Evans, C. K., Xie, W., Dill-Macky, R. and Mirocha, C. J. (2000). Biosynthesis of deoxynivalenol in
668 spikelets of barley inoculated with macronidia of *Fusarium graminearum. Plant Disease.* 84(6):
669 654-660. doi: 10.1094/PDIS.2000.84.6.654.
670 16. Fan, J., Urban, M., Parker, J. E., Brewer, H. C., Kelly, S. L., Hammond-Kosack, K. E. *et al.* (2013).
671 Characterization of the sterol 14α-demethylases of *Fusarium graminearum* identifies a novel
672 genus-specific CYP51 function. *New Phytologist*. 198(3), 821–835. doi: 10.1111/nph.12193.

673 17. Fernandez, J. and Orth, K. (2018). Rise of a cereal killer: The biology of *Magnaporthe oryzae*
674 biotrophic growth. *Trends in Microbiology*. 26(7), 582-597. doi: 10.1016/j.tim.2017.12.007.
675 18. Gao, Q., Zhao, M., Li, F., Gau, Q., Xing, S. and Wang, W. (2008). Expansins and coleoptile
676 elongation in wheat. *Protoplasma.* **233**: 73-81. doi: 10.1007/s00709-008-0303-1.
677 19. Gardiner, D. M., Kazan, K. and Manners, J. M. (2009). Nutrient profiling reveals potent inducers
678 of trichothecene biosynthesis in *Fusarium graminearum*. *Fungal Genetics and Biology.* 46, 604–
679 613. doi: 10.1016/j.fgb.2009.04.004.
680 20. Gardiner, D. M., Osbourne, S., Kazan, K. and Manners, J. M. (2009). Low pH regulates the
681 productions of deoxynivalenol by *Fusarium graminearum*. *Microbiology.* 155(9), 3149-3156. doi:
682 10.1099/mic.0.029546-0.
683 21. Guenther, J. C. and Trail, F. (2005). The development and differentiation of *Gibberella zeae*
684 (anamorph: *Fusarium graminearum*) during colonization of wheat. *Mycologia*. 97(1), 229-237.
685 doi: 10.1080/15572536.2006.11832856.
686 22. Hallen-Adams, H.E., Wenner, N., Kuldau, G. A. and Trail, F. (2011). Deoxynivalenol biosynthesis-
687 related gene expression during wheat kernel colonization by *Fusarium graminearum.*
688 *Phytopathology.* 101(9): 1091-1096. doi: 10.1094/PHYTO-01-11-0023.
689 23. Hohn, T. M., McCormick, S. P. and Desjardins, A. E. (1993). Evidence for a gene cluster involving
690 trichothecene-pathway biosynthetic genes in *Fusarium sporotrichioides*. *Current Genetics.* 24,
691 291-295. doi: 10.1007/bf00336778.
692 24. Ilgen, P., Hadeler, B., Maier, F. J. and Schäfer, W. (2009). Developing Kernel and Rachis Node
693 Induce the Trichothecene Pathway *of Fusarium graminearum* During Wheat Head Infection.
694 *Molecular Plant Microbe Interactions*, 22(8), 899-908. doi: 10.1094/MPMI-22-8-0899.
695 25. Jansen, C., von Wettstein, D., Schäfer, W., Kogel, K-H., Felk, A., and Maier, F. J. (2005). Infection
696 patterns in barley and wheat spikes inoculated with wild-type and trichodiene synthase gene
697 disrupted *Fusarium graminearum*. *PNAS.* 102(46), 16892- 16897. Doi:
698 10.1073/pnas.0508467102.

26. Kashyap, A., Planas-Marquès, M., Capellades, M., Valls, M. and Coll, N. S. (2021). Blocking intruders: inducible physico-chemical barriers against plant vascular wilt pathogens. *Journal of Experimental Botany.* 72(2): 184-198. doi: 10.1093/jxb/eraa444.

27. Lee, J. and Lu, H. (2011). Plasmodesmata: the battleground against intruders. *Trends in Plant Science*. 16(4): 201-210. doi: 10.1016/j.tplants.2011.01.004.

28. Lemmens, M., Scholz, U., Berthiller, F., Dall'Asta, C., Koutnik, A., Schuhmacher, R. *et al.* (2005). The ability to detoxify the mycotoxin deoxynivalenol colocalizes with a major quantitative trait locus for Fusarium Head Blight resistance in wheat. *Molecular Plant Microbe Interactions*. 18(12), 1318-1324. doi: 10.1094/MPMI-18-131.

29. McCormick, S. P., Stanley, A. M., Stover, N. A. and Alexander, N. J. (2011). Trichothecenes: from simple to complex mycotoxins. *Toxins*. 3(7), 802-814. doi: 10.3390/toxins3070802.

30. McMullen, M., Bergstrom, G., De Wolf, E., Dill-Macky, R., Hershman, D., Shaner, G. *et al.* (2012). A unified effort to fight an enemy of wheat and barley: Fusarium head blight. *Plant Disease*. 96(12), 1712-1728. doi: 10.1094/PDIS-03-12-0291.

31. McMullen, M., Jones, R. and Gallenburg, D. (1997). Scab of wheat and barley: a re-emerging disease of devastating impact. *Plant Disease*. 81(12), 1340 – 1348. doi: 10.1094/PDIS.1997.81.12.1340.

32. Mendiburu, F. and Yaseen, M. (2020). Agricolae: statistical procedures for agricultural research. R package version 1.4.0.

33. Mesterházy, A. (1995). Types and components of resistance to *Fusarium* head blight of wheat. *Plant Breeding.* 114, 377-386. doi: 10.1111/j.1439-0523.1995.tb00816.x

34. Mitra, P.P. and Loque. D. (2014). Histochemical staining of *Arabidopsis thaliana* secondary cell wall elements. *Journal of Visualized Experiments.* 87: 51381. doi: 10.3791/51381.

35. Parry, D.W., Jenkinson, P. and McLeod, L. (1995). Fusarium ear blight (scab) in small grain cereals—A review. *Plant Pathology*. 44, 207–238. doi: doi.org/10.1111/j.1365-3059.1995.tb02773.x.

724 36. Pestka, J. J. (2008). Mechanisms of Deoxynivalenol-Induced Gene Expression and Apoptosis. *Food*
725 *Additives and Contamination Part A: Chemistry, Analysis, Control, Exposure and Risk Assessment.*
726 25(9): 1128–1140. doi: 10.1080/02652030802056626.
727 37. Pestka, J. J. (2010). Deoxynivalenol: mechanisms of action, human exposure, and toxicological
728 relevance. *Archives of Toxicology*. 84, 663-679. doi: 10.1007/s00204-010-0579-8.
729 38. Pritsch, C., Muehlbauer, G. J., Bushnell, W. R., Somers, D. A., and Vance, C. P. (2000). Fungal
730 development and induction of defense response genes during early infection of wheat spikes by
731 *Fusarium graminearum*. *Molecular Plant Microbe Interactions.* 13(2): 159-169. doi:
732 10.1094/MPMI.2000.13.2.159.
733 39. Proctor, R. H., Hohn, T. M. and McCormick, S. P. (1995). Reduced virulence of *Gibberella zeae*
734 caused by disruption of a trichothecene toxin biosynthetic gene. *Molecular Plant Microbe*
735 *Interactions.* 8(4), 593-601. doi: 10.1094/mpmi-8-0593.
736 40. Qui, H., Zhao, X., Fang, W., Wu, H., Abubakar, Y. S., Lu, G. *et al*. (2019). Spatiotemporal nature of
737 *Fusarium graminearum*-wheat coleoptile interactions. *Phytopathology Research.* 1, article 26.
738 doi: 10.1186/s42483-019-0033-7.
739 41. Sager, R. E. and Lee, J. (2018). Plasmodesmata at a glance. *Journal of Cell Science.* 131(11),
740 jcs209346. doi: 10.1242/jcs.209346.
741 42. Sakulkoo, W., Oses-Ruiz M., Garcia E. O., Soanes, D. M., Littlejohn, G. R., Hacker, C. *et al.* (2018).
742 A single fungal MAP kinase controls plant cell-to-cell invasion by the rice blast fungus. *Science.*
743 359(6382), 1399-1403. doi: 10.1126/science.aaq0892.
744 43. Shin, S., Torres-Acosta, J.A., Heinen, S.J., McCormick, S., Lemmens, M., Paris, M. P. K., Berthiller,
745 F., Adam, G. and Muehlbauer, G. J. (2012). Transgenic *Arabidopsis thaliana* expressing a barley
746 UDP-glucosyltransferase exhibit resistance to the mycotoxin deoxynivalenol. *Journal of*
747 *Experimental Biology.* **63**(13): 4731-4740. doi: 10.1093/jxb/ers141.
748 44. Tokai, T., Koshino, H., Takahashi-Ando, N., Sato, M., Fujimura, M. and Kimura, M. (2007).
749 *Fusarium Tri4* encodes a key multifunctional cytochrome P450 monooxygenase for four

750 consecutive oxygenation steps in trichothecene biosynthesis. *Biochemical and Biophysical*
751 *Research Communications.* 353(2): 412-417. doi: 10.1016/j.bbrc.2006.12.033.
752 45. Van Der Plank, J. E. (1963). Plant diseases: epidemics and control. Academic Press, New York.
753 46. Vaughan, M., Backhouse, D. and Ponte, E. M. D. (2016). Climate change impacts on the ecology
754 of *Fusarium graminearum* species complex and susceptibility of wheat to Fusarium head blight:
755 a review. *World Mycotoxin Journal,* 9(5), 685–700. doi: 10.3920/WMJ2016.2053
756 47. Wang, Z., Yang, B., Zheng, W., Wang, L., Cai, X., Yang, J. *et al.* (2022). Recognition of glycoside
757 hydrolase 12 proteins by the immune receptor RXEG1 confers *Fusarium* head blight resistance in
758 wheat. *Plant Biotechnology Journal*. 21(4): 769-781. doi: 10.1111/pbi.13995.
759 48. Wanjiru, W. M., Zhensheng, K., and Buchenauer, H. (2002). Importance of cell wall degrading
760 enzymes produced by *Fusarium graminearum* during infection of wheat heads. *European Journal*
761 *of Plant Pathology*. 108: 803-810. doi: 10.1023/A:1020847216155.
762 49. Wickham, H. (2016). *ggplot2: Elegant Graphics for Data Analysis*. Springer-Verlag, New York.
763 50. Wilson, R. A. and Talbot, N. J. (2009). Under pressure: investigating the biology of plant infection
764 by *Magnaporthe oryzae. Nature Reviews Microbiology,* 7, 185-195. doi: 10.1038/nrmicro2032.
765 51. Wu, S., Kumar, R., Iswanto, A. B. B, and Kim, J. (2018). Callose balancing at plasmodesmata.
766 *Journal of Experimental Botany*. 69(22), 5325-5339. doi: 10.1093/jxb/ery317.
767 52. Zhang, X-W., Jia, L-J., Zhang, Y., Li, X., Zhang, D. and Tang, W-H. (2012). In planta stage-specific
768 fungal gene profiling elucidates the molecular strategies of *Fusarium graminearum* growing
769 inside wheat coleoptiles. *Plant Cell.* 24(12). 5159-5176. doi: 10.1105/tpc.112.105957.

770 # Supplementary

771 **S1 Determination of the DON concentration to be used in point inoculations with *F. graminearum***
772 **conidia (text)**

773 **S2 Toxicity of DON on plant tissue (figure)**

774 **S3 Primers used in this study (5'-3') (table)**

775 **S4 Perithecia formation *in vitro* does not require DON (text)**

776 **S5 Cell wall thickness of adaxial cell layer in resin samples (figure)**

777 **S6 Immunofluorescence detection of callose in sectioned floral tissues (figure)**

778 **S7 Quantification of immuno-labelled callose deposits in wheat spikelet resin sections (figure)**

779 **S8 Phloroglucinol staining of infected spikelets for the detection of lignin (figure)**

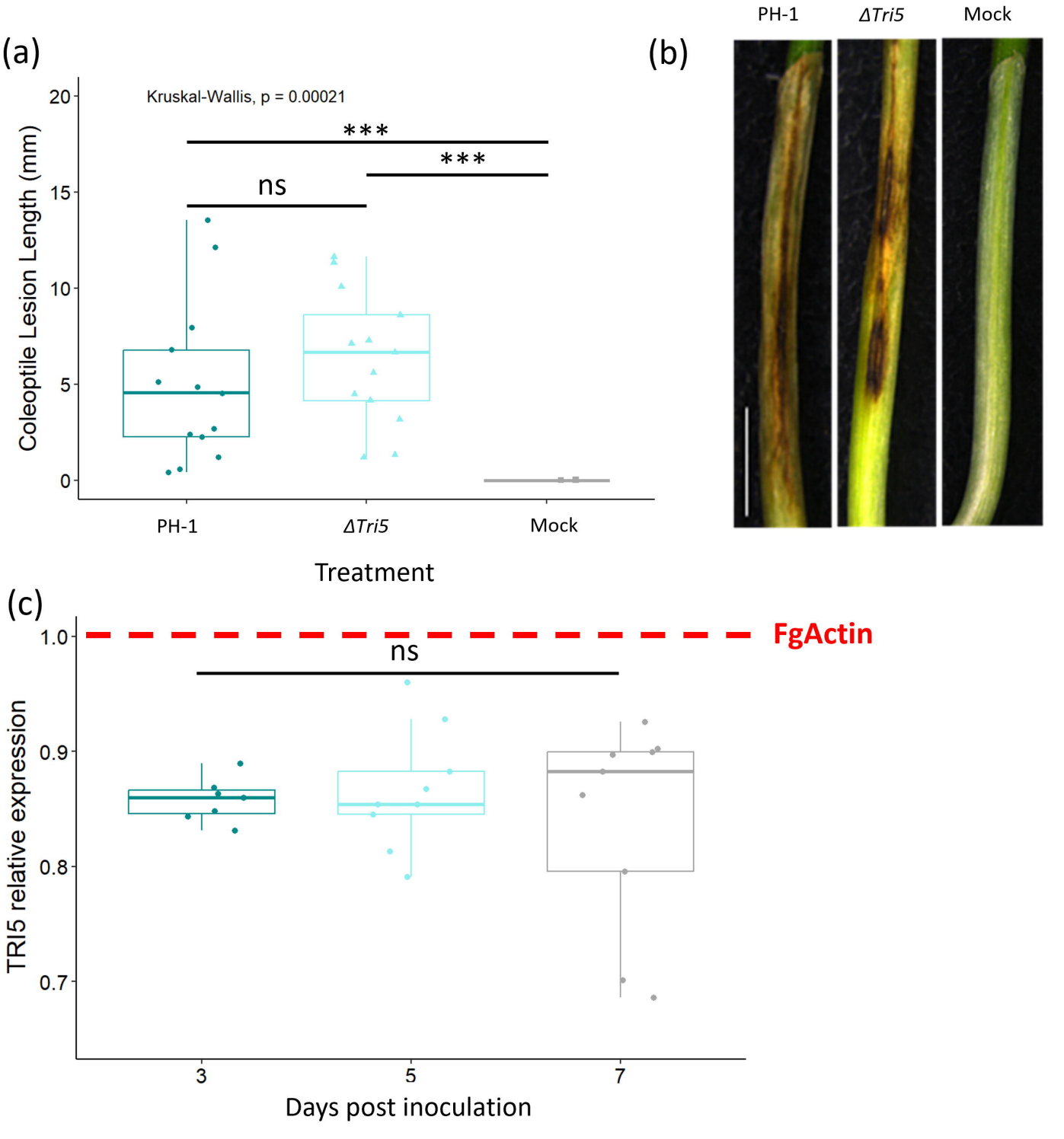
(a)
Kruskal-Wallis, p = 0.00021
***
***
ns
Coleoptile Lesion Length (mm)
20
15
10
5
0
PH-1
ΔTri5
Mock
Treatment
(b)
PH-1
ΔTri5
Mock
(c)
FgActin
ns
TRI5 relative expression
1.0
0.9
0.8
0.7
3
5
7
Days post inoculation

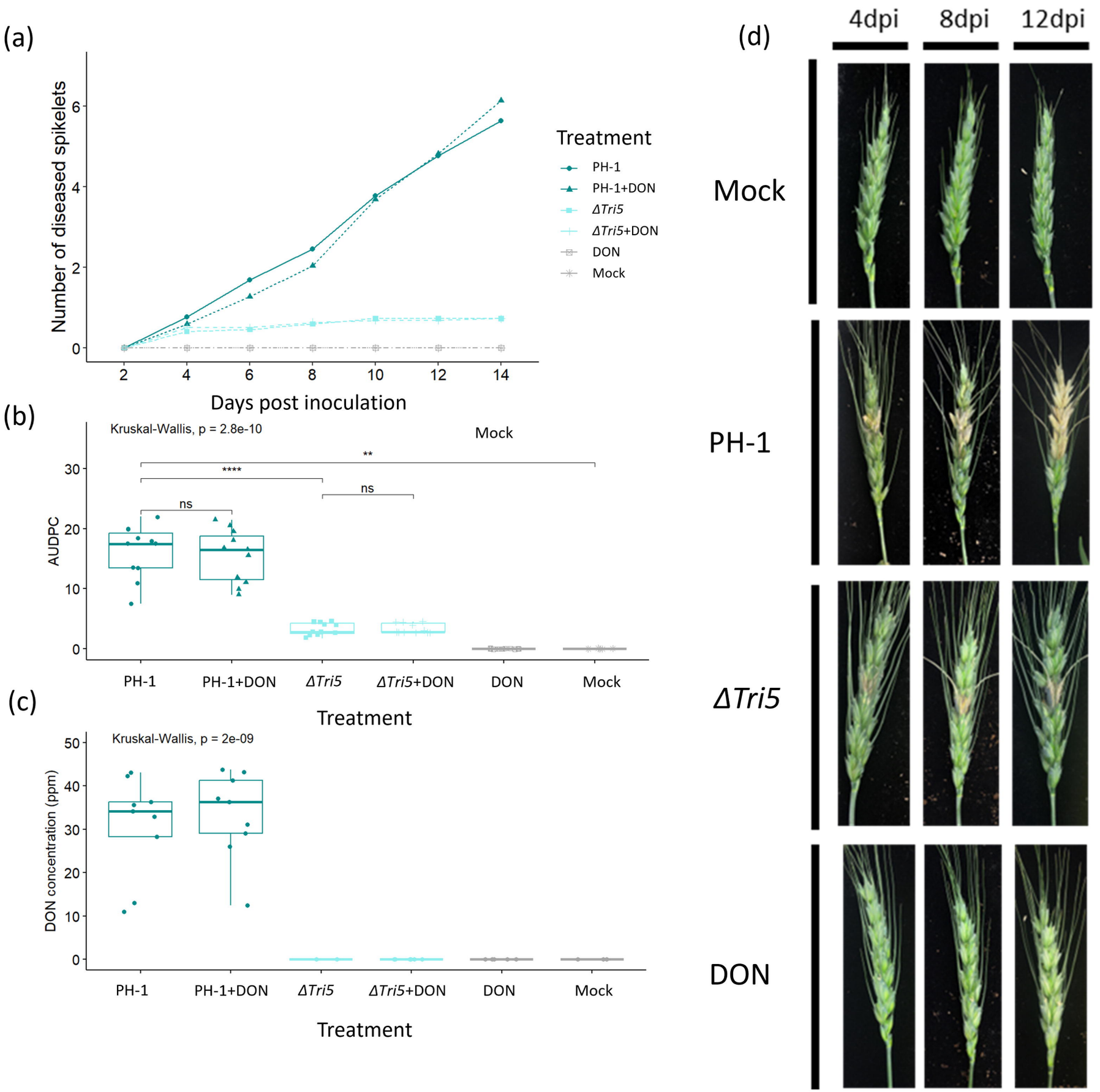
(a)
Number of diseased spikelets
Days post inoculation
Treatment
PH-1
PH-1+DON
ΔTri5
ΔTri5+DON
DON
Mock
(b)
Kruskal-Wallis, p = 2.8e-10
Mock
AUDPC
ns
****
ns
**
PH-1
PH-1+DON
ΔTri5
ΔTri5+DON
DON
Mock
Treatment
(c)
Kruskal-Wallis, p = 2e-09
DON concentration (ppm)
PH-1
PH-1+DON
ΔTri5
ΔTri5+DON
DON
Mock
Treatment
(d)
4dpi
8dpi
12dpi
Mock
PH-1
ΔTri5
DON

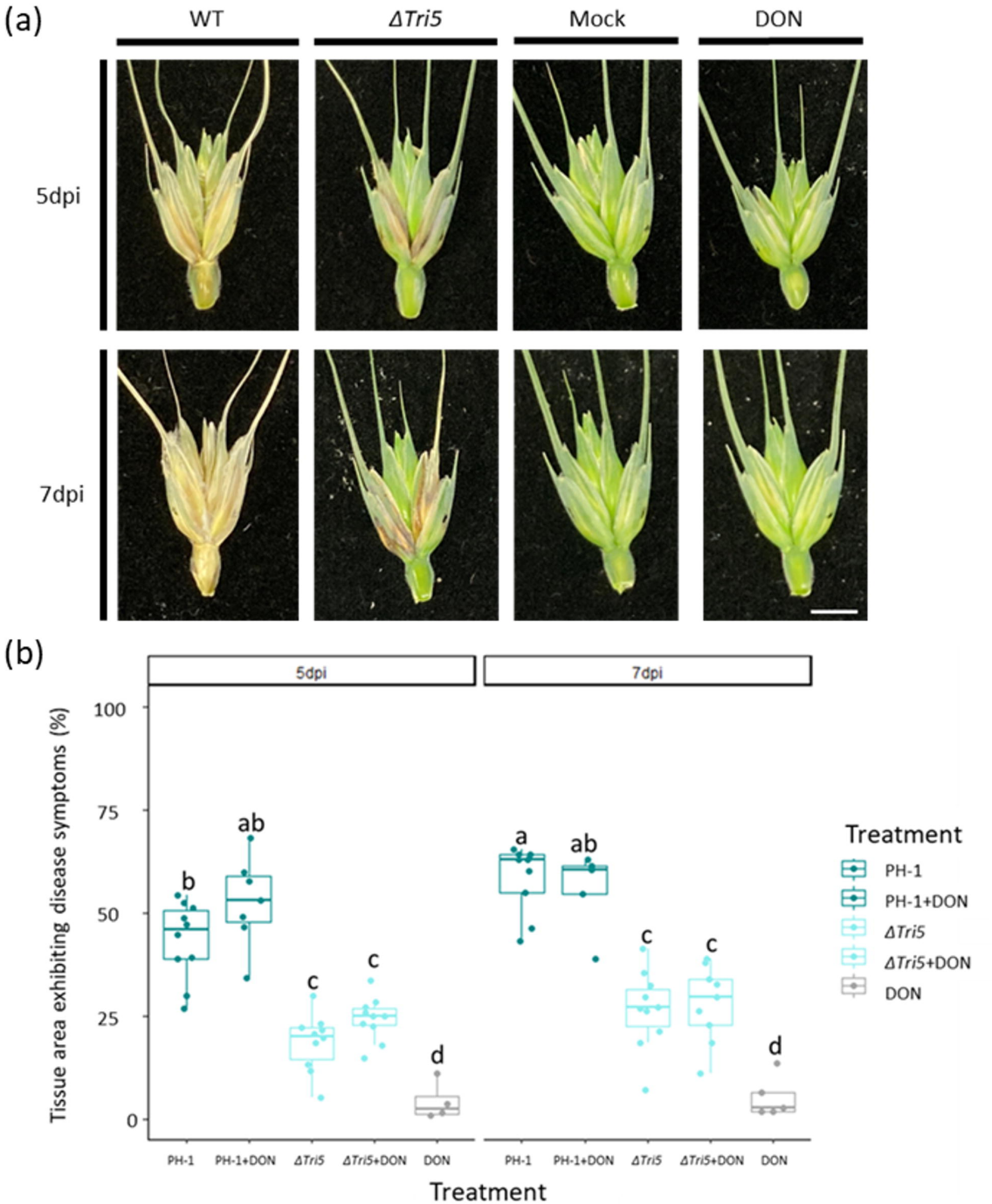
(a)
WT
ΔTri5
Mock
DON
5dpi
7dpi
(b)
5dpi
7dpi
Tissue area exhibiting disease symptoms (%)
100
75
50
25
0
b
ab
c
c
d
a
ab
c
c
d
PH-1
PH-1+DON
ΔTri5
ΔTri5+DON
DON
Treatment
Treatment
PH-1
PH-1+DON
ΔTri5
ΔTri5+DON
DON

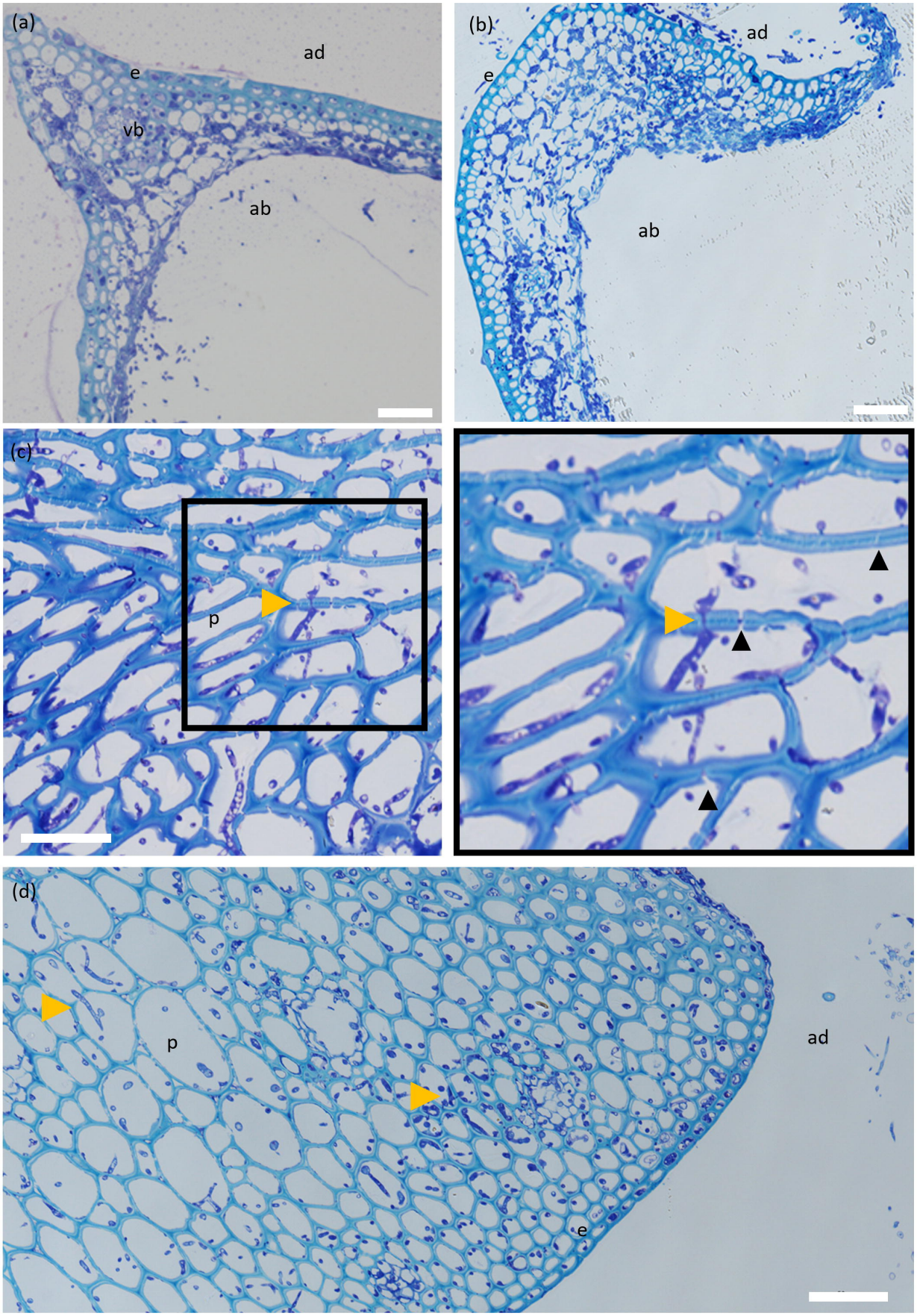
(a)
ad
e
vb
ab
(b)
ad
e
ab
(c)
p
(d)
p
ad
e

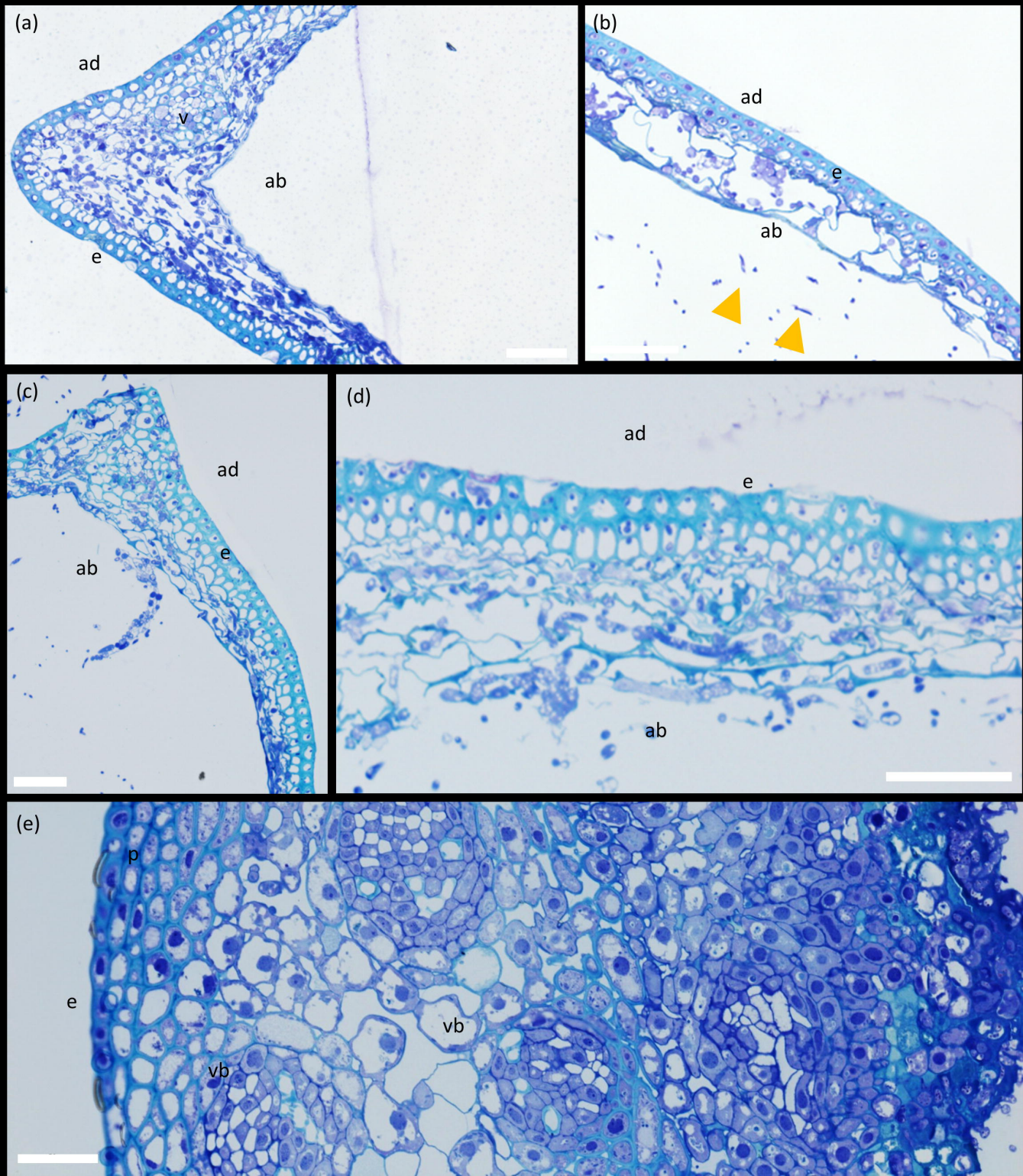
(a)
ad
v
ab
e
(b)
ad
e
ab
(c)
ad
e
ab
(d)
ad
e
ab
(e)
p
e
vb
vb

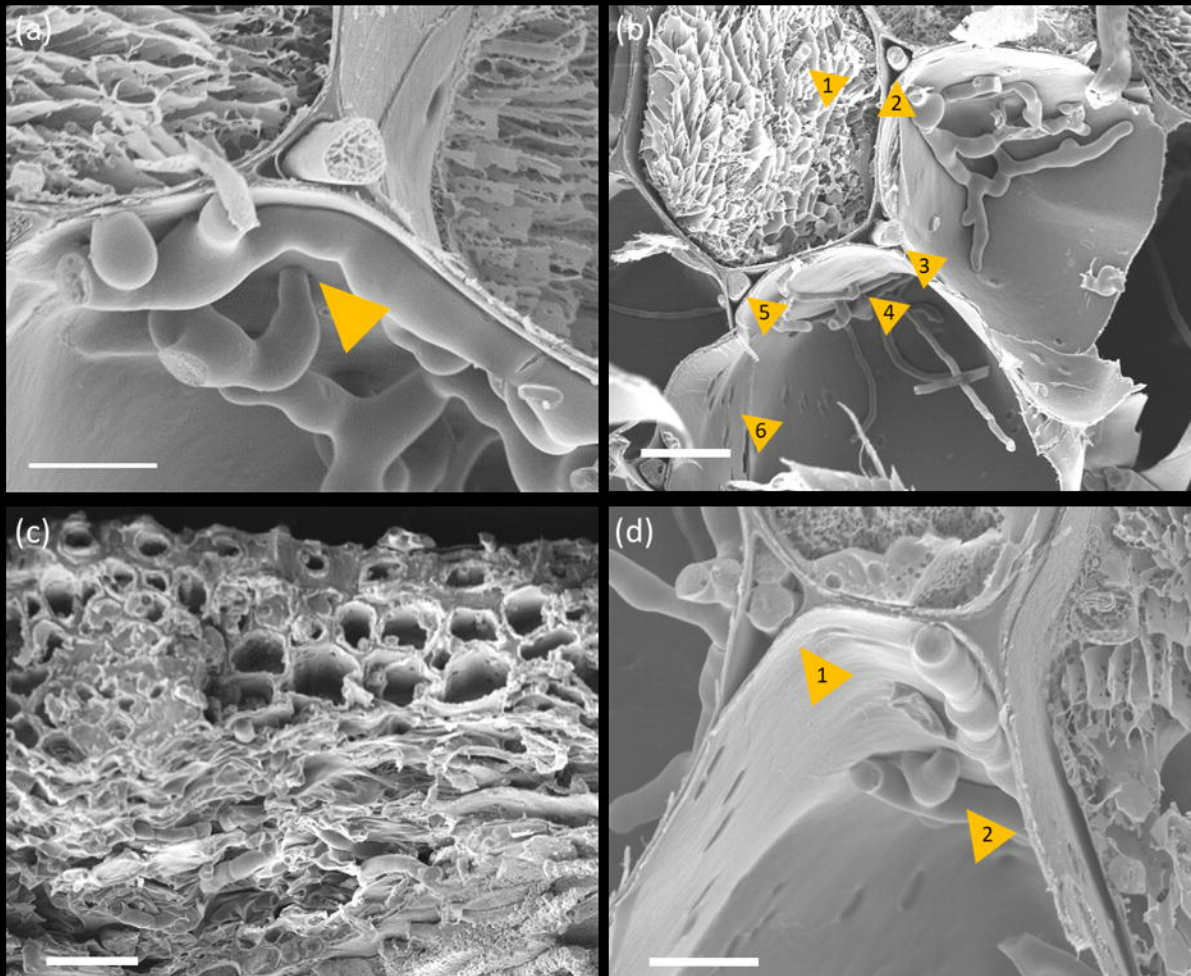
(a)
(b)
1
2
3
4
5
6
(c)
(d)
1
2

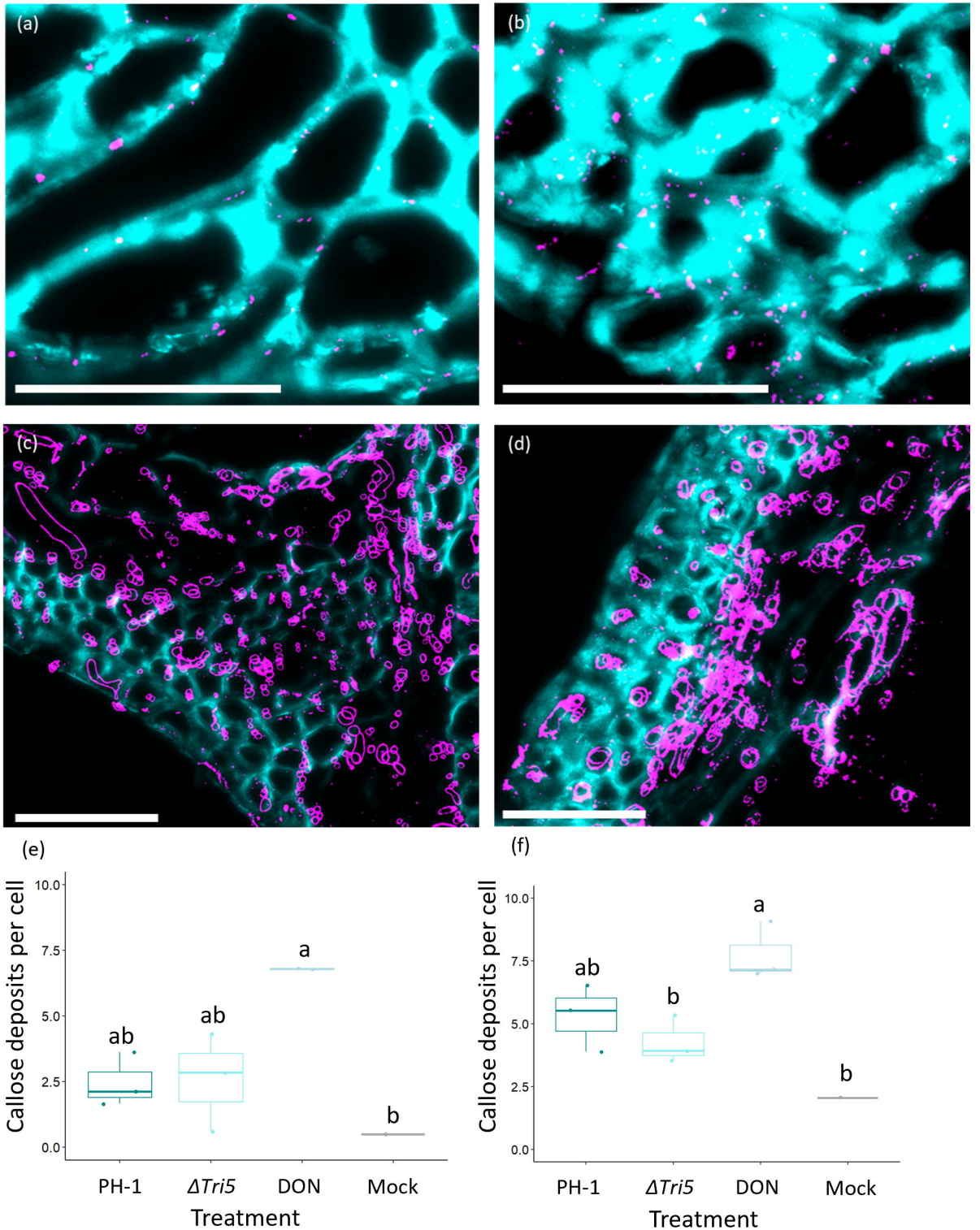
(a)
(b)
(c)
(d)
(e)
(f)
Callose deposits per cell
10.0
7.5
5.0
2.5
0.0
ab
ab
a
b
PH-1
ΔTri5
DON
Mock
Treatment
Callose deposits per cell
10.0
7.5
5.0
2.5
0.0
ab
b
a
b
PH-1
ΔTri5
DON
Mock
Treatment

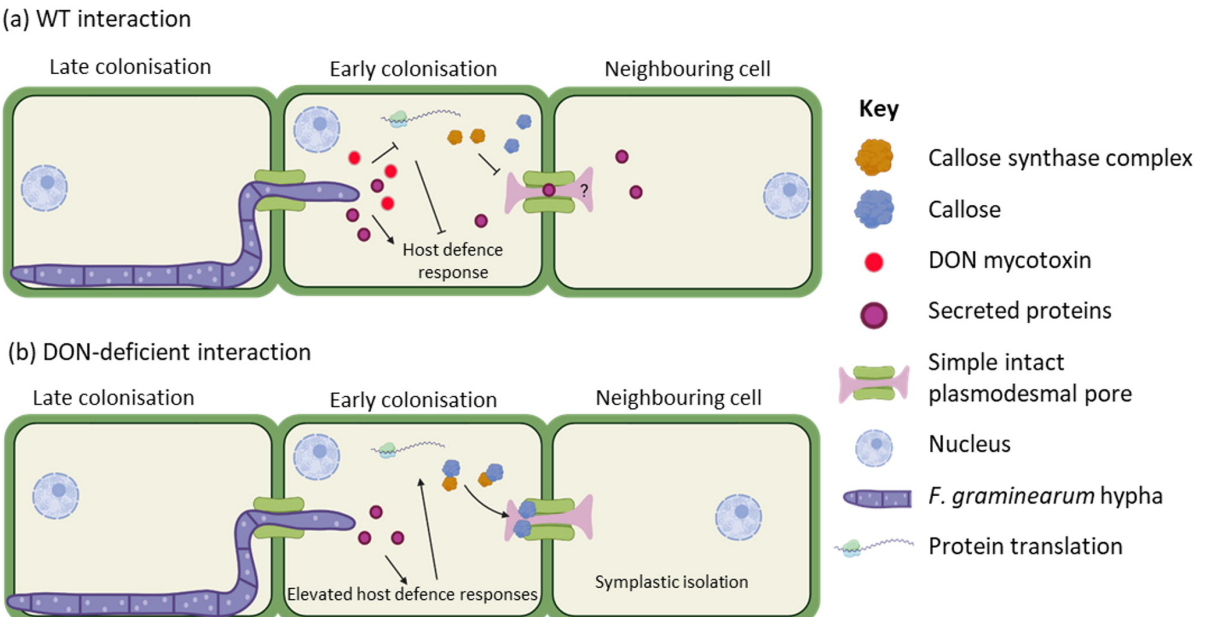
(a) WT interaction
Late colonisation
Early colonisation
Neighbouring cell
?
Host defence response
(b) DON-deficient interaction
Late colonisation
Early colonisation
Neighbouring cell
Elevated host defence responses
Symplastic isolation
Key
Callose synthase complex
Callose
DON mycotoxin
Secreted proteins
Simple intact plasmodesmal pore
Nucleus
F. graminearum hypha
Protein translation